Disorder-induced topological superconductivity in a spherical quantum-Hall–superconductor hybrid

Koji Kudo, Ryota Nakai, and Kentaro Nomura
Department of Physics, Kyushu University, Fukuoka 819-0395, Japan

(Received 22 January 2024; revised 2 July 2024; accepted 9 July 2024; published 19 July 2024)

Quantum-Hall–superconductor hybrids have been predicted to exhibit various types of topological order, providing possible platforms for intrinsically fault-tolerant quantum computing. In this paper, we investigate disorder effects on the Rashba-coupled quantum-Hall system combined with the type-II superconductor. By diagonalizing the Bogoliubov–de Gennes Hamiltonian projected into a Rashba-coupled Landau level, we demonstrate the emergence of a topological superconducting phase resulting from disorders and proximity-induced pairing. Distinctive gapless modes appear in the real-space entanglement spectrum, which is consistent with topological superconductivity. Historically, the spherical geometry has been commonly used for identifying topologically ordered states, especially quantum-Hall physics, due to its compact and contractible nature. Motivated by this, we develop a formulation to construct this hybrid system on a sphere. Our numerical demonstrations are all performed on the spherical geometry.

DOI: 10.1103/PhysRevB.110.035147

I. INTRODUCTION

The topology of the many-body configuration space determines possible quantum statistics of particles [1]. The fundamental group of the configuration space is the symmetry group in three or higher dimensions while it is the braid group in two dimensions, allowing exotic particles beyond bosons and fermions, namely anyons [2]. The emergence of anyonic quasiparticles is a defining feature of topological order [3], which has revealed a new aspect of phases of matter beyond the scope of Landau's theory. Typical examples of topologically ordered states are the fractional quantum-Hall (FQH) effect [4–6], quantum spin liquids [7–10], and $p+ip$ superconductors (SCs) [11,12]. Recent progress in experiments for anyons has been made, for example, through measurements of the half-integer quantized thermal Hall conductivity in the Kitaev materials [13–15] and detections of the fractional statistics via directly braiding the FQH quasiparticles [16–18]. Creating, manipulating, and reading non-Abelian anyons are basic elements for topological quantum computing [19–21], which has been an ultimate goal in condensed matter physics.

A key strategy for generating non-Abelian anyon platforms has involved designing topological materials. Hybridizing well-understood ingredients, even if they are not inherently topological, has proved to be a valuable tool in this process, leveraging their interplay to introduce topological order. For instance, hybridization with s-wave nontopological SCs induces superconducting proximity effects, leading to Majorana modes on surfaces of strong topological insulators [22,23], spin-orbit coupled semiconductors [24–27], quantum anomalous Hall systems [28], and integer quantum-Hall (IQH) systems [29–31]. Recent efforts have been directed towards exploring hybrid quantum-Hall–SC (QH-SC) systems that host much more exotic particles such as parafermions [32–41] and Fibonacci anyons [42–46] (the so-called QH superconductivity [47–67] also exhibits similar physics as the QH-SC hybrids). These developments have highlighted the potential of QH-SC hybrids for universal topological quantum computation.

In theoretical exploration of topological order, the geometry of systems is quite crucial. Particularly, boundaries introduce low-energy modes as edge states [68,69], rendering compact surfaces suitable for investigating bulk properties of topologically ordered states. On a compact surface with genus $g \geqslant 1$, the one-dimensional unitary representation of the braid group is absent. Consequently, states on such surfaces must be degenerate to form a multicomponent structure [70–75], referred to as topological degeneracy [76,77]. This phenomenon, while intriguing and closely related to the topological nature of anyons, can pose technical challenges in numerical studies. Indeed, the spherical geometry [78] with $g=0$ has been commonly used in the FQH physics.

Based on this background, our paper discusses two topics: (i) investigating disorder effects on hybrid QH-SC systems and (ii) developing a formulation for hybrid QH-SC systems with the spherical geometry. Specifically, we consider the Rashba-coupled IQH system combined with the type-II SCs, motivated by Refs. [30,31]. In addition, we incorporate random distributions of δ-function impurities. Figure 1 visually represents our model. The type-II SC is chosen because of the strong magnetic field required for the QH system. Our numerical studies demonstrate that the interplay between disorders and proximity-induced pairing results in a topological superconducting phase associated with the half-integer Chern number. Here, we refer to the half of the Bogoliubov–de Gennes (BdG) Chern number (namely the Chern number of BdG bands) as the "Chern number." We identify this phase by detecting gap-closing lines. The entanglement spectrum reveals distinctive gapless modes, providing further evidence for topological superconductivity. Our numerical calculations are all performed on the spherical geometry.

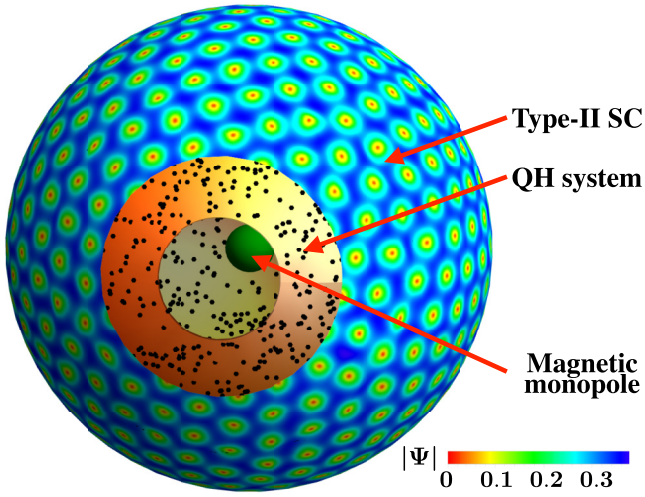

FIG. 1. QH–SC hybrid on a sphere. The outer (inner) surface represents the type-II SC (QH system). The color of the outer surface indicates the order parameter $|\Psi|$ at $2\bar{Q} = 450$. We normalize Ψ as $\int d\bar{\Omega}|\Psi|^2 = 1$ for simplicity. The black dots in the inner surface depict impurities, with a total count of 4500. The order (outer or inner) of each system is not significant. The green sphere at the center is the magnetic monopole.

The paper is organized as follows. In Sec. II, we review two components in our hybrid system on a sphere: the Rashba-coupled QH system and a model type-II SC. In Sec. III, we derive the BdG Hamiltonian projected into a Rashba-coupled LL with the spherical geometry. Section IV presents numerical results and the paper concludes in Sec. V.

II. SETUP FOR THE SPHERICAL GEOMETRY

A. Rashba-coupled Landau level

We begin by considering the Rashba-coupled Landau level (LL) structure. The single-particle Hamiltonian reads $H_1 = \vec{\pi}^2/2m_e - \alpha_R(\vec{\sigma} \times \vec{\pi})_z$, where $\vec{\pi}$ is the canonical momentum, m_e is the electron mass, $\vec{\sigma}$ is the Pauli matrices, and α_R is the Rashba coupling strength. In the planar geometry, this reduces to [30,31,79–83]

$$H_1 = \hbar\omega_c \begin{pmatrix} a^\dagger a + \frac{1}{2} & -ig_R a \\ ig_R a^\dagger & a^\dagger a + \frac{1}{2} \end{pmatrix}, \tag{1}$$

where $\omega_c = eB/m_e c$ is the cyclotron frequency, B is the strength of the magnetic field, and $g_R = \sqrt{2}\alpha_R/l_B\omega_c$, with $l_B = \sqrt{\hbar c/eB}$ the magnetic strength. The ladder operator is defined by $a^\dagger = (\pi_x + i\pi_y)l_B/\sqrt{2}\hbar$. Within the subspace,

$$\Phi_{nm} = \left[\begin{pmatrix} |n-1, m\rangle \\ 0 \end{pmatrix}, \begin{pmatrix} 0 \\ |n, m\rangle \end{pmatrix} \right] \quad \text{with } n \geqslant 1, \tag{2}$$

where $|n, m\rangle$ is the eigenstate of angular momentum $\hbar m$ in the nth LL without spin-orbit coupling, the Hamiltonian H_1 is block-diagonalized as

$$\Phi^\dagger_{nm} H_1 \Phi_{nm} = \hbar\omega_c \begin{pmatrix} n - \frac{1}{2} & -ig_R\sqrt{n} \\ ig_R\sqrt{n} & n + \frac{1}{2} \end{pmatrix}. \tag{3}$$

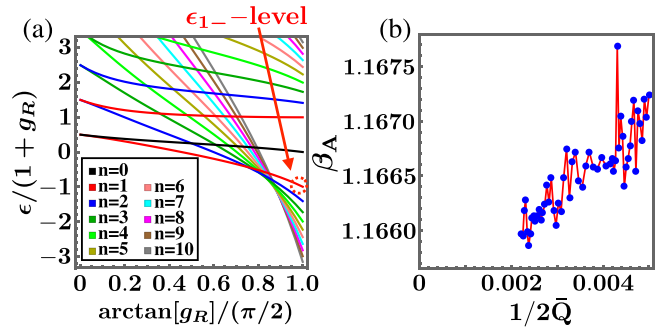

FIG. 2. (a) Rashba-coupled LLs ϵ_0 and $\epsilon_{n\pm}$ with $n \leqslant 10$. At $g_R \sim 0$ and ∞, the energy is quantized in increments of n and $\sqrt{n}$, respectively. We will use the ϵ_{1-} level, represented by a red circle, for the QH-SC hybrid systems. (b) Abrikosov factor β_A at various $2\bar{Q}$'s. These values are computed by numerically minimizing the GL free energy $\mathcal{F}$.

Its eigenvalues and eigenvectors are

$$\epsilon_{n\pm} = \hbar\omega_c\left(n \pm \sqrt{1/4 + g_R^2 n}\right),$$
$$\vec{v}_{n\pm} = \begin{pmatrix} i/2 \mp i\sqrt{g_R^2 n + 1/4} \\ g_R\sqrt{n} \end{pmatrix}/\mathcal{N}, \tag{4}$$

where $\mathcal{N}$ is a normalization factor. In addition, the unpaired state $(0, |0, m\rangle)$ is an eigenstate of H_1 with energy $\epsilon_0 = \hbar\omega_c/2$. In the limit $g_R \to \infty$, H_1 reduces to the Hamiltonian of massless Dirac fermions. Figure 2(a) shows the single-particle energy $\epsilon_{n\pm}$. To observe the evolution for $g_R \in [0, \infty)$, we scale the energy by $1 + g_R$ and plot it as a function of $\arctan(g_R)$. At $g_R \sim 0$, the energy is quantized in increments of n while in increments of $\sqrt{n}$ at $g_R \sim \infty$. In the next section, we will focus on the Rashba-coupled LL with ϵ_{1-}, referred to as the ϵ_{1-} level. This is the lowest energy level for $0 < g_R < \sqrt{6}$ and becomes the "$n = -1$ LL" of the two-dimensional Dirac Hamiltonian [84] as g_R approaches infinity.

In the following, we consider Haldane's spherical geometry [78], where N particles move on the surface under a radial magnetic field. The total radial flux is $2Q\phi_0$, where $\phi_0 = hc/e$ is the flux quantum and $2Q$ is an integer. In the spinless problem without spin-orbit coupling, single-particle states are labeled by the orbital angular momentum l and its z-component m because of rotational symmetry. Their possible values are $l = |Q|, |Q| + 1, \ldots$ and $m = -l, -l + 1, \ldots, l$. The $2l + 1$ states with $l = |Q| + n$ correspond to the nth LL. The eigenstates are the monopole harmonics $Y_{Qlm}(\vec{\Omega})$ [85,86], where $\vec{\Omega}$ represents the angular coordinates θ and ϕ.

Spin-orbit coupling is not straightforward to apply as it mixes different LLs having different degrees of degeneracy on a sphere. The same issue also arises, e.g., in the QH physics in graphene [87–92]. Fortunately, because of the non-flat geometry, relativistic electrons on a Haldane's sphere with physical fluxes Q are subject to different magnetic fluxes $Q_\pm = Q \pm 1/2$ depending on the spin orientation [93–96]. As a result, nth LL with Q_+ and $(n + 1)$th LL with Q_- have the same degree of degeneracy. Based on this solution, we use the

following basis, instead of Eq. (2), for the spherical geometry:

$$\Phi_{Qnm} = \left[\begin{pmatrix} Y_{Q_+,Q_++n,m} \\ 0 \end{pmatrix}, \begin{pmatrix} 0 \\ Y_{Q_-,Q_++n,m} \end{pmatrix}\right]. \tag{5}$$

The labels n, m represent the Landau index and the angular momentum.

B. Abrikosov vortex lattice

We now review a model type-II superconductor on a sphere [97,98] to calculate the superconducting order parameter, which we will use to construct the proximity-induced pairing amplitude in our hybrid system below. Here we consider a clean system with a magnetic field slightly smaller than the upper critical field H_{c2}. A magnetic monopole is placed at the center of the sphere in the same fashion as above. For clarity, we mark quantities for Cooper pairs by a bar; superconducting flux quantum $\bar{\phi}_0 = hc/\bar{e}$ with $\bar{e} = 2e$ and the total flux $2\bar{Q}\bar{\phi}_0$ (equivalently, $\bar{Q} = 2Q$).

To identify the superconducting order parameter, we consider the GL free energy $\mathcal{F}[\Psi] = \int d\vec{\Omega}\, f[\Psi]$ with

$$f[\Psi] = -a|\Psi|^2 + \frac{b}{2}|\Psi|^4 + \frac{1}{2\bar{m}_e}\left|\left(\frac{\hbar}{i}\vec{\nabla} + \frac{\bar{e}}{c}\vec{A}\right)\Psi\right|^2 + \frac{|\vec{B}|^2}{8\pi}, \tag{6}$$

where a, b are phenomenological parameters ($a, b > 0$). We now demonstrate that Ψ minimizing $\mathcal{F}$ does not depend on a and b except the overall amplitude. For simplicity, we assume that the order parameter lies in the lowest LL of Cooper pairs [99] as

$$\Psi(\vec{\Omega}) = \sum_{\bar{m}=\bar{Q}}^{\bar{Q}} u_{\bar{m}} Y_{\bar{Q}\bar{Q}\bar{m}}(\vec{\Omega}), \tag{7}$$

and one obtains

$$-a\int d\vec{\Omega}|\Psi|^2 = -a\vec{u}^\dagger\vec{u}, \tag{8}$$

$$\frac{b}{2}\int d\vec{\Omega}|\Psi|^4 = \frac{b}{2}\sum_{s=-2\bar{Q}}^{2\bar{Q}} |\vec{u}^T K^{(s)}\vec{u}|^2, \tag{9}$$

where $\vec{u} = (u_{-\bar{Q}}, u_{-\bar{Q}+1}, \ldots, u_{\bar{Q}})$ and

$$K^{(s)}_{ij} = S\begin{pmatrix} \bar{Q} & \bar{Q} & -2\bar{Q} \\ \bar{Q} & \bar{Q} & 2\bar{Q} \\ i & j & -i-j \end{pmatrix}\delta_{s,i+j}, \tag{10}$$

$$S\begin{pmatrix} Q_1 & Q_2 & Q_3 \\ l_1 & l_2 & l_3 \\ m_1 & m_2 & m_3 \end{pmatrix} \equiv \int d\vec{\Omega}\, Y_{Q_1 l_1 m_1} Y_{Q_2 l_2 m_2} Y_{Q_3 l_3 m_3}. \tag{11}$$

Dropping the constant, the GL free energy reduces to

$$\mathcal{F}(\vec{u}) = -ax + \frac{b}{2}\frac{\beta_A}{4\pi}x^2, \tag{12}$$

where $x = \vec{u}^\dagger\vec{u}$ and β_A is the Abrikosov factor:

$$\beta_A \equiv \frac{\langle|\Psi|^4\rangle}{\langle|\Psi|^2\rangle^2} = \frac{4\pi\sum_s |\vec{u}^T K^{(s)}\vec{u}|^2}{(\vec{u}^\dagger\vec{u})^2}. \tag{13}$$

Here $\langle\cdot\rangle$ represents a spatial average. Equation (13) implies that β_A is independent of $|\vec{u}|$ and also x ($= \vec{u}^\dagger\vec{u}$). The GL free energy has a peak at $x = 4\pi a/(b\beta_A) \equiv x_0$ and its value is

$$\mathcal{F}_{\text{peak}}(\vec{u}) = -\frac{2\pi a^2}{b\beta_A}. \tag{14}$$

Thus minimizing $\mathcal{F}$ is equivalent to minimizing β_A. Since β_A does not involve a and b, the solution of $\vec{u}$ that minimizes $\mathcal{F}$ does not either, apart from the norm (the norm of $\vec{u}$ is determined by x_0).

We numerically minimize $\mathcal{F}$ with $a = b = 1$ and calculate the Abrikosov factor β_A for various $2\bar{Q}$ in Fig. 2(b). The value of β_A with $2\bar{Q} \to \infty$ is 1.1652, determined through linear extrapolation. This is slightly larger than 1.1596 calculated on an infinite flat plane with triangular Abrikosov vortex lattices [100]. This deviation comes from the fact that a triangular lattice cannot generally cover a surface of a sphere [97]. In Fig. 1, we plot $|\Psi(\vec{\Omega})|$ on a sphere at $2\bar{Q} = 450$. The vortices basically form a triangular lattice but there are defects as well. Similar discussions can be found in the context of the famous Thomson problem [101–103] and the Wigner crystal in the QH problem [104].

We use the solution of $\vec{u}$ to construct a proximity-induced pairing amplitude in our hybrid system below. In Fig. 2(b), we minimize $\mathcal{F}$ with M_{sample} different initial points of $\vec{u}$ with $80 \leqslant M_{\text{sample}} \lesssim 400$. We then plot β_A if the lowest β_A is at least threefold degenerate. Here, two β_A's are considered the same if their difference is less than 10^{-8}. In Fig. 2(b), after consecutively changing Q from 100 to 119 to make sure that there is no particular Q dependency (e.g., an even-odd effect), we pick every three from 120 to 225. (We failed to seek β_A that satisfies this criterion at some values of $\bar{Q}$).

III. SPHERICAL HYBRID SYSTEM

Our spherical hybrid system is composed of a Rashba-coupled QH system with disorders and a type-II s-wave SC. Hybridization induces the superconducting proximity effect on the QH system. The type-II SC is chosen due to the strong magnetic field needed for the QH system. We write its total Hamiltonian as

$$\mathcal{H} = \int d\vec{\Omega}\, c^\dagger(\vec{\Omega})[H_1(\vec{\Omega}) + H_{\text{imp}}(\vec{\Omega}) - \mu]c(\vec{\Omega}) + \int d\vec{\Omega}\, c^\dagger_\uparrow(\vec{\Omega})\Delta(\vec{\Omega})c^\dagger_\downarrow(\vec{\Omega}) + \text{H.c.}, \tag{15}$$

where $c^\dagger = (c^\dagger_\uparrow, c^\dagger_\downarrow)$, $c^\dagger_\sigma(\vec{\Omega})$ is the creation operator for a fermion with spin σ, and μ is a chemical potential. Here, H_1 describes the Rashba-coupled LLs as discussed in the previous section and H_{imp} represents a random distribution of $2N_{\text{imp}} = 20Q$ impurities at positions $\vec{\Omega}_i$ with the energy $\pm w$:

$$H_{\text{imp}}(\vec{\Omega}) = \sum_{i=1}^{2N_{\text{imp}}} (-1)^i w\delta^2(\vec{\Omega} - \vec{\Omega}_i). \tag{16}$$

The factor $(-1)^i$ is multiplied to adjust the average energy to zero. The impurities broaden the LLs and their width is estimated to be $\Gamma = (w/R^2)\sqrt{4\rho/2\pi l_B^2}$, where $R = l_B\sqrt{Q}$ and $\rho = 2N_{\text{imp}}/4\pi R^2$, by using the self-consistent Born approximation [105]. We parametrize the strength of disorders by Γ

rather than w below. The pairing amplitude $\Delta(\vec{\Omega})$ in Eq. (15) is defined by

$$\Delta(\vec{\Omega}) = C \sum_{\bar{m}=-\bar{Q}}^{\bar{Q}} u_{\bar{m}} Y_{\bar{Q}\bar{Q}\bar{m}}(\vec{\Omega}), \tag{17}$$

where C is a constant and $u_{\bar{m}}$ is the solution of the minimizing problem of the GL free energy $\mathcal{F}$ discussed above. We parametrize the strength of the proximity effect by $\Delta_0 = \sqrt{|C|^2 \vec{u}^\dagger \vec{u}/(4\pi)}$, which corresponds to the spatial average of $\Delta(\vec{\Omega})$, i.e.,

$$\int d\vec{\Omega} |\Delta(\vec{\Omega})|^2 = 4\pi \Delta_0^2. \tag{18}$$

Now, we assume that (i) the chemical potential μ is close to the ϵ_{1-} level and (ii) the Landau gap $\hbar\omega_c$ significantly exceeds both disorder and proximity effect. These validate projection of the Hilbert space onto the ϵ_{1-} level subspace. The total projected Hamiltonian has the form of

$$\mathcal{H}_{\rm BdG} = \frac{1}{2} \boldsymbol{f}^\dagger H_{\rm BdG} \boldsymbol{f}, \tag{19}$$

$$H_{\rm BdG} = \begin{pmatrix} h_0 & 2D \\ 2D^\dagger & -h_0^* \end{pmatrix}, \tag{20}$$

where $\boldsymbol{f}^\dagger = (f^\dagger_{-Q_+}, \ldots, f^\dagger_{Q_+}, f_{-Q_+}, \ldots, f_{Q_+})$ and $f^\dagger_m$ is the creation operator of states in the ϵ_{1-} level defined by

$$f^\dagger_m = (d^\dagger_{Q_+ Q_+ m\uparrow}, d^\dagger_{Q_- Q_+ m\downarrow}) \vec{v}_{1-}, \tag{21}$$

$$d^\dagger_{Q_\pm lm\sigma} = \int d\vec{\Omega}\, Y_{Q_\pm lm}(\vec{\Omega}) c^\dagger_\sigma(\vec{\Omega}), \tag{22}$$

where $\vec{v}_{1-}$ was defined in Eq. (4). Here, $Q_\pm$ in Eq. (22) takes Q_+ (Q_-) with spin $\sigma = \uparrow$ ($\downarrow$) and $Q_\pm$ was defined as $Q_\pm = Q \pm 1/2$ in Sec. II A. The explicit forms of matrices h_0, D are derived in Appendix A.

As shown in Appendix A, the matrix D is proportional to $g_R/\sqrt{1+4g_R^2} \equiv \gamma(g_R)$, where again g_R parametrizes the Rashba coupling strength. In other words, the pairing amplitude Δ_0 can be rescaled by $\gamma(g_R)$ [30,31]. $\gamma(g_R)$ is a monotonically increasing function, with $\gamma(0) = 0$ and $\gamma(\infty) = 1/2$, indicating that the spin-orbit coupling generates and enhances the proximity-induced superconducting pairing. For simplicity, we set $\gamma = 1/2$ (equivalently $g_R \to \infty$) in the following numerical calculation, but results for any value of g_R can be read off by appropriately rescaling Δ_0.

Now, let us consider the eigenvalue problem of the projected Hamiltonian $H_{\rm BdG}$ in Eq. (20) as

$$H_{\rm BdG} \begin{pmatrix} u_k \\ v_k \end{pmatrix} = E_k \begin{pmatrix} u_k \\ v_k \end{pmatrix}, \tag{23}$$

where u_k and v_k are N-dimensional vectors, $2N \equiv 4Q_+ + 2$ is the dimension of $H_{\rm BdG}$, and k is just the label of eigenvalues, which we arrange in ascending order as $E_{-(N-1/2)} \leqslant E_{-(N-1/2)+1} \leqslant \cdots \leqslant E_{N-1/2}$. The particle-hole symmetry brings $E_{-k} = -E_k$ and $\begin{pmatrix} u_{-k} \\ v_{-k} \end{pmatrix} = \begin{pmatrix} v_k^* \\ u_k^* \end{pmatrix}$. Then, we have

$$\mathcal{H}_{\rm BdG} = \frac{1}{2} \sum_{\text{all } k} E_k g_k^\dagger g_k = \sum_{k<0} E_k g_k^\dagger g_k + \text{const}, \tag{24}$$

where

$$g_k^\dagger = g_{-k} = \boldsymbol{f}^\dagger \begin{pmatrix} u_k \\ v_k \end{pmatrix}. \tag{25}$$

The ground state is given by $|G\rangle = \prod_{k<0} g_k^\dagger |0\rangle$ with $|0\rangle$ the vacuum state of electrons.

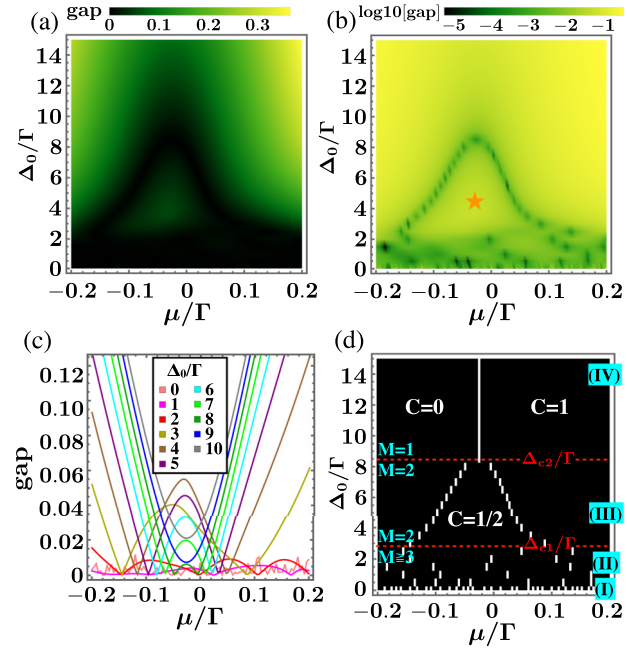

FIG. 3. (a),(b) Density plots of the energy gap and its logarithm as functions of the chemical potential μ and the pairing amplitude Δ_0, scaled by the width of the LL Γ (the "gap" is also scaled by Γ). The star in (b) indicates a topological superconducting phase. (c) Energy gap as a function of μ/Γ. (d) White points indicate the local-minimum gap. When identifying these points, we sweep μ in increments of $\delta\mu/\Gamma = 0.004$ at each Δ_0/Γ. The red dashed lines represent Δ_{c1}/Γ and Δ_{c2}/Γ, representing the boundary where the number of local-minimum gap points, M, changes. There are four regions as labeled by (I)–(IV). We set $2Q = 198$ in all of the figures.

IV. NUMERICAL RESULTS

The system parameters we have not fixed yet are

$$(2Q, \Delta_0, \Gamma, \mu).$$

The main goal now is to find a topological superconducting phase by varying Δ_0/Γ and μ/Γ. For simplicity, we measure μ relative to ϵ_{1-}. The numerical results below are all obtained by diagonalizing $\mathcal{H}_{\rm BdG}$ in Eq. (19).

A. Energy gap

Figure 3(a) plots the energy gap—the energy separation around $E = 0$ in the BdG spectrum—as a function of μ/Γ and Δ_0/Γ with $2Q = 198$, which is a "typical" value of $2Q$ as mentioned below. To visualize gap-closing points, we

present its logarithm in Fig. 3(b). The subsequent analysis suggests that the centered phase with a star in the figure is a topological superconducting phase. Figure 3(c) explicitly shows the values of the gap at specific Δ_0's, indicating that each local minimum corresponds to the gap closing as long as $0 < \Delta_0/\Gamma \lesssim 8.5$.

To clarify emergent phases, we generate Fig. 3(d) that displays local-minimum gap points. Here, we count the number of those points at each Δ_0, denoted M, and then define Δ_{c1} (Δ_{c2}) as the transition points where M changes to 2 (1) as Δ_0 increases. In Fig. 3(d), we have $\Delta_{c1}/\Gamma \sim 3$ and $\Delta_{c2}/\Gamma \sim 8.5$. Let us now discuss each of the following four regions. (The ground state at $|\mu| \gg \Delta_0, \Gamma$ is completely occupied or unoccupied states. Associating the Chern number C, we call each of them "$C = 1$" and "$C = 0$" states, respectively).

(I) $\Delta_0/\Gamma = 0$: *QH plateau transition.* A plateau transition connecting $C = 0$ and 1 phases occurs as μ is changed. Localized states induce multiple gap-closing points in Fig. 3(d).

(II) $0 < \Delta_0 < \Delta_{c1}$: *Open question.* We have $M \geqslant 3$. The nature of the gap-closing points is still an open question. There are two possible scenarios: a plateau transition connecting (1) $C = 0, 1/2$ and 1 phases or (2) $C = 0$ and 1 phases. The distinction lies in whether the intermediate state at $\mu/\Gamma \sim 0$ is a topological SC (see the next paragraph for more details) or a gapless state [30] arising from a network model with states carrying different Chern numbers. Determining the possibilities requires more careful calculations, which we leave for future study.

(III) $\Delta_{c1} < \Delta_0 < \Delta_{c2}$: *Emergence of $C = 1/2$ phase.* We have $M = 2$. Given that the intermediate phase is situated between $C = 0$ and $C = 1$ phases, we expect it to be the $C = 1/2$ phase, namely a topological superconducting phase with the unit BdG Chern number. This expectation is further supported by the entanglement spectrum calculated in the next section.

(IV) $\Delta_{c2} < \Delta_0$: *Disappearance of $C = 1/2$ phase.* We have $M = 1$. The value of the local minimum increases as Δ_0/Γ is increased; see Fig. 3(c). According to Ref. [30], the pairing amplitude induced from a mixed state SC contains point nodes akin to the $p + ip$-wave pairing potential, which gives rise to only two phases: $C = 0$ and $C = 1$. In other words, a clean system without impurities does not exhibit topological superconducting states. This suggests that the observed finite minimum gap at $\Delta_0/\Gamma = 9, 10$ is a finite-size effect and therefore the line in Fig. 3(d) can be interpreted as the phase boundary dividing $C = 0$ and 1.

B. Entanglement spectrum

Now we topologically characterize the $C = 1/2$ phase. A typical way is to calculate the Chern number, but is fundamentally challenging in our model due to the absence of translation invariance in the spherical geometry. Cutting the system and counting Majorana edge modes will allow detection of the $C = 1/2$ phase but is also technically hard. (The $C = 1/2$ state will exhibit one edge mode in the BdG spectrum).

Instead, we calculate the single-particle real-space entanglement spectrum (EtS) [106–114]. The EtS exhibits a qualitatively similar structure as the eigenvalues of the single-particle correlation function [106], which holds true even in the BdG formulation [114] (see Appendix B). Henceforth, we refer to the eigenvalues of the correlation function as the EtS. The EtS characterizes a topological nature of systems. If a two-dimensional system is topologically trivial, the EtS are concentrated on 0 and 1 and exhibit little dispersion. Conversely, in systems like the Chern insulator or the IQH system, additional eigenvalues emerge, crossing 0 and 1 akin to midgap states in the EtS. Leveraging this observation, we explore phases carrying the nonzero Chern number within our system.

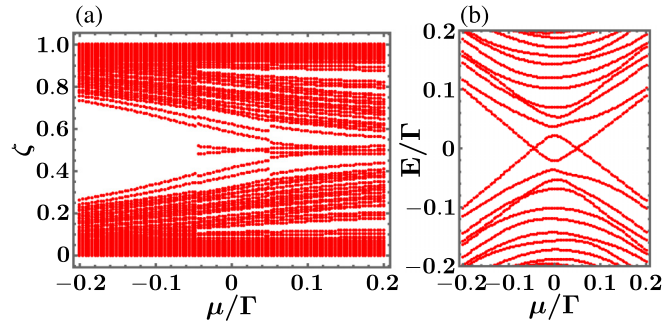

FIG. 4. (a) Entanglement spectrum (EtS). When $\mu/\Gamma \lesssim -0.05$, EtS is relatively concentrated around 0 and 1. At $\mu/\Gamma \sim -0.05$, the midgap states suddenly appear and the density of ζ's between 0 and 1 is increased as μ/Γ is increased. (b) BdG spectrum. There are two gap-closing points at $\mu/\Gamma \sim \pm 0.05$.

Now, we calculate the correlation function only on the northern hemisphere (NH) in our system as

$$C_{\mathrm{NH}}(\vec{\Omega}, \vec{\Omega}') \equiv \int_{\mathrm{NH}} d\vec{\Omega}\ \langle G|\, \boldsymbol{c}(\vec{\Omega})\boldsymbol{c}^{\dagger}(\vec{\Omega}')\,|G\rangle\,, \tag{26}$$

where $\boldsymbol{c}^{\dagger} = (c_{\uparrow}^{\dagger}, c_{\downarrow}^{\dagger}, c_{\uparrow}, c_{\downarrow})$ and $|G\rangle$ is the ground state of the BdG Hamiltonian. The EtS is given by the eigenvalue problem,

$$\int_{\mathrm{NH}} d\vec{\Omega}' C(\vec{\Omega}, \vec{\Omega}')\vec{\psi}_k(\vec{\Omega}') = \zeta_k \vec{\psi}_k(\vec{\Omega}). \tag{27}$$

Appendix C describes how to get the solutions of this equation. As derived there, one obtains $\zeta_k = 0$ or 1 at $\mu/\Gamma \to -\infty$. On the other hand, the ground state at $\mu/\Gamma \to \infty$ is the IQH state, producing "entanglement gapless modes" as well that cross $\zeta_k = 0$ and 1 [110]. Below, we explore the EtS in the intermediate range of μ/Γ. Figure 4(a) illustrates the EtS as a function of μ/Γ. Here, we set $2Q = 222$ and $\Delta_0/\Gamma = 4$ because this system has the relatively large energy gap of the ground state, resulting in less finite-size effect in the EtS. In comparison, Fig. 4(b) shows the BdG spectrum, revealing two gap-closing points at $\mu/\Gamma \sim \pm 0.05$. The values of ζ's are relatively concentrated around 0 and 1 when $\mu/\Gamma \lesssim -0.05$, consistent with the trivial phase. At $\mu/\Gamma \sim -0.05$, the midgap states suddenly appear in the EtS and the density of ζ's between 0 and 1 is increased as we increase μ/Γ. This suggests that the Chern number of the ground state is nonzero when $\mu/\Gamma \gtrsim -0.05$. This observation is consistent with the fact that the region separated by the gap-closing points $-0.05 \lesssim \mu/\Gamma \lesssim 0.05$ is a superconducting phase.

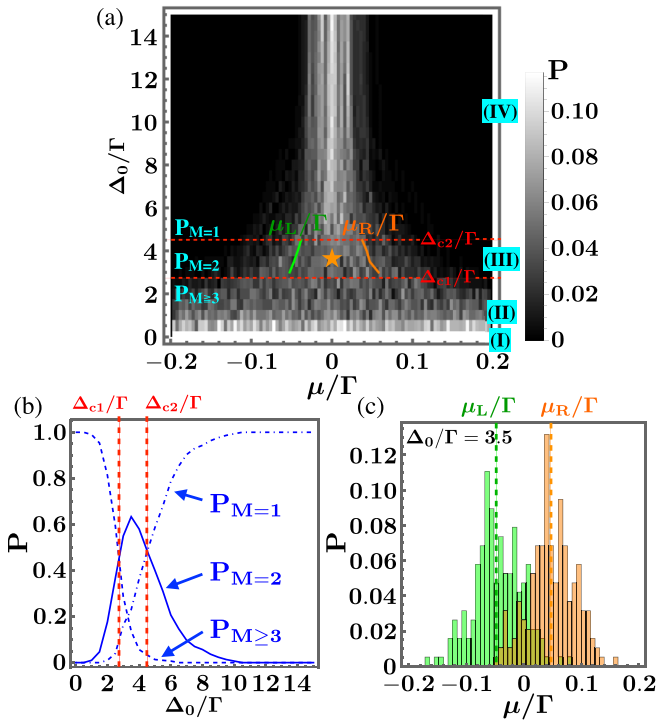

FIG. 5. (a) Distribution of local-minimum gap points. The color indicates the normalized count. The star denotes the topological superconducting regime, enclosed by two red-dashed lines (representing Δ_{c1}/Γ and Δ_{c2}/Γ) and green and orange lines (representing μ_L/Γ and μ_R/Γ). (b) Probability of having M local-minimum gap points. The values of Δ_{c1} and Δ_{c2} are deduced from intersections of each line. (c) Distribution of local-minimum gap points with $M = 2$ at $\Delta_0/\Gamma = 3.5$. The green and orange colors represent data for the left and right local-minimum gap, respectively. The values of μ_L and μ_R are defined as the means for each data set. We set $2Q = 198$ in all of the figures.

Currently, we have no further way to exactly identify the Chern number of this phase, which we leave for future study.

C. Ensemble average

So far we have discussed findings based on a single impurity distribution. In the remainder of the work, we will present results using multiple random distributions.

Figure 5(a) is an analog of Fig. 3(d) but incorporates 300 random distributions of impurities. This is a 2D histogram where the gray color represents the normalized count of local-minimum-gap samples at each point. The superconducting phase is expected to emerge in $\Delta_{1c} < \Delta_0 < \Delta_{2c}$ and $\mu_L < \mu < \mu_R$ as indicated by a star. Each phase boundary is identified as follows: Fig. 5(b) plots the probability of having M local-minimum gap points, denoted P_M, as a function of Δ_0/Γ. We define Δ_{c1} (Δ_{c2}) by intersections of $P_{M\geqslant 3}$ and $P_{M=2}$ ($P_{M=2}$ and $P_{M=1}$). We determine μ_R and μ_L using histograms as in Fig. 5(c), where the green (orange) bars represent the distribution of left (right) local-minimum gap points. We define μ_L and μ_R as means for each data set. To explore the thermodynamic limit, we calculate Δ_{c1}/Γ and Δ_{c2}/Γ for different $2Q$'s in the above way and present the results in Fig. 6. The dashed lines indicate the mean values of each data set. The

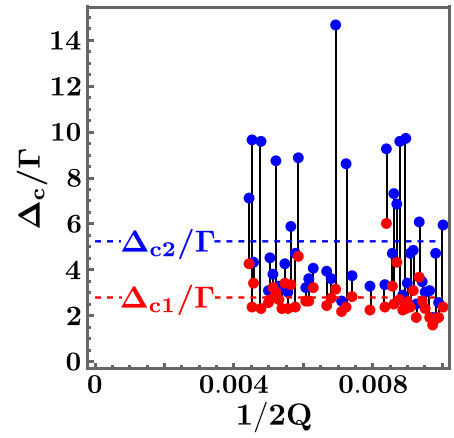

FIG. 6. Size-scaling analysis for Δ_{c1}/Γ (red dots) and Δ_{c2}/Γ (blue dots). The black lines connect the red and the blue dots at each $2Q$. The dashed lines represent the average of each data set.

difference $\Delta_{c2}/\Gamma - \Delta_{c1}/\Gamma$ appears to remain finite as systems increase in size, suggesting the presence of the topological superconducting phase in the thermodynamic limit. We have chosen $2Q = 198$ in Figs. 3 and 5 as a representative example because it is the largest $2Q$ within the five closest systems to the two dashed lines.

V. CONCLUDING REMARKS

In this paper, we formulate a scheme to combine the Rashba-coupled QH system with a type-II s-wave SC on the spherical geometry. Through this setup, we numerically demonstrate the emergence of a disorder-induced phase between a trivial and the IQH phases. We expect this to be the superconducting phase associated with the half-integer Chern number. This expectation is further supported by revealing the entanglement gapless modes in the EtS.

Our spherical model will be a useful platform for future study on topological order. Although we have focused on the (Rashba-coupled) IQH system, our formulation is also valid for the FQH system. The interplay between fractionalization and superconductivity can give rise to intriguing phenomena such as $\mathbb{Z}_n$ parafermions or Fibonacci anyons as mentioned in the Introduction. The topological degeneracy of such states, stemming from their non-Abelian nature, is generally not exact in a finite system, which can lead to subtle problems in, for example, assessing degeneracy or energy excitations in a translationally invariant system. Our spherical model inherently avoids this issue, facilitating the straightforward identification of non-Abelian topological order.

ACKNOWLEDGMENTS

We acknowledge the computational resources offered by Research Institute for Information Technology, Kyushu University. The work is supported in part by JSPS KAKENHI Grants No. JP23K19036 and No. JP20H01830 and JST CREST Grant No. JPMJCR18T2.

APPENDIX A: EXPLICIT FORMS OF h_0 AND D

1. Matrix h_0

The matrix h_0 is derived from the first term of $\mathcal{H}$ in Eq. (15). Within the ϵ_{1-}-level space, we can perform the following replacement:

$$c^\dagger_\sigma(\vec{\Omega}) \to \sum_{m=l}^{l} Y^*_{Q_\pm lm}(\vec{\Omega}) d^\dagger_{Q_\pm lm\sigma}, \tag{A1}$$

$$(d^\dagger_{Q_+Q_+m\uparrow}, d^\dagger_{Q_-Q_+m\downarrow}) \to f^\dagger_m \vec{v}^\dagger_{1-}. \tag{A2}$$

Then the disorder potential is expressed by

$$\int d\vec{\Omega}\, c^\dagger(\vec{\Omega}) H_{\rm imp}(\vec{\Omega}) c(\vec{\Omega}) = \sum_{m,m'=-Q_+}^{Q_+} W_{mm'} f^\dagger_m f_m, \tag{A3}$$

where

$$\begin{aligned} W_{mm'} &= |[\vec{v}_{1-}]_\uparrow|^2 W_{Q_+}(Q_+m; Q_+m') \\ &\quad + |[\vec{v}_{1-}]_\downarrow|^2 W_{Q_-}(Q_+m; Q_+m'), \\ W_Q(lm; l'm') &= w(-1)^{Q-m'} \sum_{l''=l_i}^{l_f} \\ &\quad \times S \begin{pmatrix} -Q & Q & 0 \\ l & l' & l'' \\ -m & m' & m-m' \end{pmatrix} \\ &\quad \times \sum_{i=1}^{2N_{\rm imp}} (-1)^i Y_{l''m'-m}(\vec{\Omega}_i), \end{aligned} \tag{A4}$$

where $l_i = \max\{|l-l'|, |m-m'|\}$ and $l_f = l + l'$. Noting that H_1 becomes an identity matrix with a prefactor ϵ_{1-}, one gets

$$(h_0)_{mm'} = W_{mm'} + \delta_{mm'}(\epsilon_{1-} - \mu). \tag{A5}$$

2. Matrix D

The pairing amplitude is deformed as

$$\begin{aligned} \int d\vec{\Omega}\, c^\dagger_\uparrow(\vec{\Omega}) \Delta(\vec{\Omega}) c^\dagger_\downarrow(\vec{\Omega}) &= \sum_{ll'} \sum_{mm'} \Delta(Q_+lm; Q_-l'm') \\ &\quad \times d^\dagger_{Q_+lm\uparrow} d^\dagger_{Q_-l'm'\downarrow}, \end{aligned} \tag{A6}$$

where

$$\begin{aligned} &\Delta(Q_+lm; Q_-l'm') \\ &= \int d\vec{\Omega}\, Y^*_{Q_+lm} Y^*_{Q_-l'm'} \Delta(\vec{\Omega}) \\ &= C u_{m+m'} (-1)^{\bar{Q}-m-m'} S \begin{pmatrix} -Q_+ & -Q_- & \bar{Q} \\ l & l' & \bar{Q} \\ -m & -m' & m+m' \end{pmatrix}. \end{aligned} \tag{A7}$$

Note the validity of the replacement $d^\dagger_{Q_+lm\uparrow} d^\dagger_{Q_-l'm'\downarrow} \to (\gamma/i) f^\dagger_m f^\dagger_{m'}$ within the ϵ_{1-} level, where $\gamma \equiv i[\vec{v_{1-}}]^*_1 [\vec{v_{1-}}]^*_2 = g_R/\sqrt{1+4g_R^2}$. The matrix elements of D, denoted $D_{mm'}$, are given by

$$D_{mm'} = \frac{\gamma}{i} \Delta(Q_+Q_+m; Q_-Q_+m'). \tag{A8}$$

One can easily show $D^T = -D$.

APPENDIX B: ENTANGLEMENT SPECTRUM AND CORRELATION FUNCTION IN THE BDG FORMULATION

The EtS is determined from the properties of the correlation functions. In this Appendix, we review this using a quadratic BdG Hamiltonian as $(1/2)\sum_{ij} \boldsymbol{a}^\dagger_i H_{ij} \boldsymbol{a}_j$ with $\boldsymbol{a}^\dagger_i = (a^\dagger_i, a_i)$ on a lattice, where spin or orbital indices can be added along with the spatial coordinate i. By dividing the system into two parts, A and B, the entanglement Hamiltonian $\mathcal{H}_A$ is defined by

$$\rho_A \equiv {\rm tr}_B \rho = \frac{1}{Z} e^{-\mathcal{H}_A}, \tag{B1}$$

where $\rho = |G\rangle\langle G|$ with $|G\rangle$ the ground state, ${\rm tr}_B$ refers to the trace over the region B, and Z is a normalization constant. The entanglement Hamiltonian also has a quadratic form as $\mathcal{H}_A = (1/2)\sum_{ij\in A} \boldsymbol{a}^\dagger_i (H_A)_{ij} \boldsymbol{a}_j$ [106]. The matrix H_A can be expressed using the correlation function matrix $(C_A)_{i,j\in A} = {\rm tr}[\rho_A \boldsymbol{a}_i \boldsymbol{a}^\dagger_j]$ as [106,107,114]

$$C_A = \frac{1}{1+e^{-H_A}}. \tag{B2}$$

Since the spectra of H_A and C_A have the qualitatively same structure, we focus on C_A and refer to its eigenvalues ζ'_ks as the EtS in the main text. The particle-hole symmetry $PH_AP^{-1} = -H_A$ leads to

$$PC_AP^{-1} = 1 - C_A, \tag{B3}$$

where P is an antiunitary matrix. Because of $0 \leqslant \zeta_k \leqslant 1$, the EtS is symmetric with respect to $1/2$. Assuming the validity of applying the above discussion to a continuum system, we consider the correlation function in Eq. (26).

APPENDIX C: EIGENVALUES OF $C_{\rm NH}$

In this Appendix, we describe how to numerically solve the eigenvalue problem in Eq. (27). The correlation function $C_{\rm NH}$ reduces to

$$C_{\rm NH}(\vec{\Omega}, \vec{\Omega}') = \delta(\vec{\Omega}, \vec{\Omega}') + Y(\vec{\Omega}) A Y^\dagger(\vec{\Omega}'). \tag{C1}$$

Here, δ, Y, and A are the matrices defined as

$$\delta(\vec{\Omega}, \vec{\Omega}') \equiv \begin{pmatrix} \delta^2(\vec{\Omega}-\vec{\Omega}') & & & \\ & \delta^2(\vec{\Omega}-\vec{\Omega}') & & \\ & & 0 & \\ & & & 0 \end{pmatrix}, \tag{C2}$$

$$Y = \begin{pmatrix} \boldsymbol{Y}_{Q_+Q_+} & & & \\ & \boldsymbol{Y}_{Q_-Q_+} & & \\ & & \boldsymbol{Y}^*_{Q_+Q_+} & \\ & & & \boldsymbol{Y}^*_{Q_-Q_+} \end{pmatrix}, \tag{C3}$$

$$A = \begin{pmatrix} -M_u M_u^\dagger & -M_u M_v^\dagger \\ M_u^* M_v^T & M_u^* M_u^T \end{pmatrix}, \tag{C4}$$

where

$$\boldsymbol{Y}_{Ql}(\vec{\Omega}) = (Y_{Ql-l}(\vec{\Omega}), \ldots, Y_{Qll}(\vec{\Omega})), \tag{C5}$$

$$M_u = \vec{v}_{1-} \otimes u, \tag{C6}$$

$$M_v = \vec{v}^*_{1-} \otimes v. \tag{C7}$$

Here, $\otimes$ refers to the tensor product and (u, v) are defined as

$$\begin{aligned} u &\equiv (u_{-(N-1/2)}, \ldots, u_{-1/2}), \\ v &\equiv (v_{-(N-1/2)}, \ldots, v_{-1/2}), \end{aligned} \tag{C8}$$

where u_k and v_k are elements of eigenvectors of H_{BdG} as defined in Eq. (23).

Let us write the eigenvalue equation in Eq. (27) again:

$$\int_{\mathrm{NH}} d\vec{\Omega}' C(\vec{\Omega}, \vec{\Omega}')\vec{\psi}_k(\vec{\Omega}') = \zeta_k \vec{\psi}_k(\vec{\Omega}).$$

By expanding $\vec{\psi}_k(\vec{\Omega}) = Y(\vec{\Omega})\vec{\alpha}_k$ and operating $\int d\vec{\Omega}\, Y^\dagger(\vec{\Omega})$ from the left, Eq. (27) reduces to

$$(\delta' - AB)\vec{\alpha}_k = \zeta_k \vec{\alpha}_k, \tag{C9}$$

where

$$B = \int_{\mathrm{NH}} d\vec{\Omega}\, \vec{Y}^\dagger \vec{Y}, \tag{C10}$$

$$\delta' = \mathrm{diag}\{\mathbf{1}_{4Q_+ + 2}, \mathbf{0}_{4Q_+ + 2}\}, \tag{C11}$$

with $\mathbf{1}_n$ ($\mathbf{0}_n$) the n-dimensional identity (zero) matrices. Although $\delta' - AB$ is not Hermitian, Eq. (C9) can be transformed to a Hermitian problem as

$$(\delta' - B^{1/2}AB^{1/2})\vec{\alpha}'_k = \zeta_k \vec{\alpha}'_k, \tag{C12}$$

where $\vec{\alpha}'_k = B^{1/2}\vec{\alpha}_k$. We note that A is Hermitian and $B = \mathrm{diag}\{B_\uparrow, B_\downarrow, B_\uparrow, B_\downarrow\}$, with $(B_\sigma)_{mm'} = \delta_{mm'} \int_{\mathrm{NH}} d\vec{\Omega} |Y_{Q_\pm Q_+ m}|^2$ being positive-definite (this integration reduces to the beta function). At $\mu/\Gamma \to -\infty$, A becomes a zero matrix because $u = 0$, leading to ζ_k being 0 or 1. On the other hand, the ground state at $\mu/\Gamma \to \infty$ is the IQH state, producing "entanglement gapless modes" that cross $\zeta_k = 0$ and 1 [110].

[1] Y.-S. Wu, Phys. Rev. Lett. **52**, 2103 (1984).
[2] F. Wilczek, Phys. Rev. Lett. **49**, 957 (1982).
[3] X.-G. Wen, Adv. Phys. **44**, 405 (1995).
[4] D. C. Tsui, H. L. Stormer, and A. C. Gossard, Phys. Rev. Lett. **48**, 1559 (1982).
[5] R. B. Laughlin, Phys. Rev. Lett. **50**, 1395 (1983).
[6] J. K. Jain, *Composite Fermions* (Cambridge University Press, New York, 2007).
[7] V. Kalmeyer and R. B. Laughlin, Phys. Rev. Lett. **59**, 2095 (1987).
[8] M. A. Levin and X.-G. Wen, Phys. Rev. B **71**, 045110 (2005).
[9] A. Kitaev, Ann. Phys. (NY) **321**, 2 (2006).
[10] G. Jackeli and G. Khaliullin, Phys. Rev. Lett. **102**, 017205 (2009).
[11] N. Read and D. Green, Phys. Rev. B **61**, 10267 (2000).
[12] D. A. Ivanov, Phys. Rev. Lett. **86**, 268 (2001).
[13] Y. Kasahara, T. Ohnishi, Y. Mizukami, O. Tanaka, S. Ma, K. Sugii, N. Kurita, H. Tanaka, J. Nasu, Y. Motome *et al.*, Nature (London) **559**, 227 (2018).
[14] T. Yokoi, S. Ma, Y. Kasahara, S. Kasahara, T. Shibauchi, N. Kurita, H. Tanaka, J. Nasu, Y. Motome, C. Hickey *et al.*, Science **373**, 568 (2021).
[15] J. A. N. Bruin, R. R. Claus, Y. Matsumoto, N. Kurita, H. Tanaka, and H. Takagi, Nat. Phys. **18**, 401 (2022).
[16] J. Nakamura, S. Liang, G. C. Gardner, and M. J. Manfra, Nat. Phys. **16**, 931 (2020).
[17] H. Bartolomei, M. Kumar, R. Bisognin, A. Marguerite, J.-M. Berroir, E. Bocquillon, B. Plaais, A. Cavanna, Q. Dong, U. Gennser *et al.*, Science **368**, 173 (2020).
[18] J. Nakamura, S. Liang, G. C. Gardner, and M. J. Manfra, arXiv:2304.12415.
[19] A. Kitaev, Ann. Phys. (NY) **303**, 2 (2003).
[20] C. Nayak, S. H. Simon, A. Stern, M. Freedman, and S. Das Sarma, Rev. Mod. Phys. **80**, 1083 (2008).
[21] J. K. Jain, Curr. Sci. **119**, 430 (2020)
[22] L. Fu and C. L. Kane, Phys. Rev. Lett. **100**, 096407 (2008).
[23] A. R. Akhmerov, J. Nilsson, and C. W. J. Beenakker, Phys. Rev. Lett. **102**, 216404 (2009).
[24] J. D. Sau, R. M. Lutchyn, S. Tewari, and S. Das Sarma, Phys. Rev. Lett. **104**, 040502 (2010).
[25] R. M. Lutchyn, J. D. Sau, and S. Das Sarma, Phys. Rev. Lett. **105**, 077001 (2010).
[26] Y. Oreg, G. Refael, and F. von Oppen, Phys. Rev. Lett. **105**, 177002 (2010).
[27] J. Alicea, Phys. Rev. B **81**, 125318 (2010).
[28] X.-L. Qi, T. L. Hughes, and S.-C. Zhang, Phys. Rev. B **82**, 184516 (2010).
[29] B. Zocher and B. Rosenow, Phys. Rev. B **93**, 214504 (2016).
[30] R. V. Mishmash, A. Yazdani, and M. P. Zaletel, Phys. Rev. B **99**, 115427 (2019).
[31] G. Chaudhary and A. H. MacDonald, Phys. Rev. B **101**, 024516 (2020).
[32] M. Cheng, Phys. Rev. B **86**, 195126 (2012).
[33] N. H. Lindner, E. Berg, G. Refael, and A. Stern, Phys. Rev. X **2**, 041002 (2012).
[34] M. Burrello, B. van Heck, and E. Cobanera, Phys. Rev. B **87**, 195422 (2013).
[35] D. J. Clarke, J. Alicea, and K. Shtengel, Nat. Commun. **4**, 1348 (2013).
[36] A. Vaezi, Phys. Rev. B **87**, 035132 (2013).
[37] A. Milsted, E. Cobanera, M. Burrello, and G. Ortiz, Phys. Rev. B **90**, 195101 (2014).
[38] J. Klinovaja, A. Yacoby, and D. Loss, Phys. Rev. B **90**, 155447 (2014).
[39] J. Alicea and P. Fendley, Annu. Rev. Condens. Matter Phys. **7**, 119 (2016).

[40] E. Sagi, A. Haim, E. Berg, F. von Oppen, and Y. Oreg, Phys. Rev. B **96**, 235144 (2017).
[41] J. Liang, G. Simion, and Y. Lyanda-Geller, Phys. Rev. B **100**, 075155 (2019).
[42] A. Vaezi, Phys. Rev. X **4**, 031009 (2014).
[43] R. S. K. Mong, M. P. Zaletel, F. Pollmann, and Z. Papić, Phys. Rev. B **95**, 115136 (2017).
[44] Y. Hu and C. L. Kane, Phys. Rev. Lett. **120**, 066801 (2018).
[45] P. L. S. Lopes, V. L. Quito, B. Han, and J. C. Y. Teo, Phys. Rev. B **100**, 085116 (2019).
[46] O. Gül, Y. Ronen, S. Y. Lee, H. Shapourian, J. Zauberman, Y. H. Lee, K. Watanabe, T. Taniguchi, A. Vishwanath, A. Yacoby *et al.*, Phys. Rev. X **12**, 021057 (2022).
[47] Z. Tešanović, M. Rasolt, and L. Xing, Phys. Rev. Lett. **63**, 2425 (1989).
[48] A. K. Rajagopal and R. Vasudevan, Phys. Rev. B **44**, 2807 (1991).
[49] Z. Tešanović, M. Rasolt, and L. Xing, Phys. Rev. B **43**, 288 (1991).
[50] M. R. Norman, Phys. Rev. Lett. **66**, 842 (1991).
[51] H. Akera, A. H. MacDonald, S. M. Girvin, and M. R. Norman, Phys. Rev. Lett. **67**, 2375 (1991).
[52] A. K. Rajagopal and J. C. Ryan, Phys. Rev. B **44**, 10280 (1991).
[53] M. Rasolt and Z. Tešanović, Rev. Mod. Phys. **64**, 709 (1992).
[54] A. H. MacDonald, H. Akera, and M. R. Norman, Phys. Rev. B **45**, 10147 (1992).
[55] M. Norman, H. Akera, and A. MacDonald, Physica C **196**, 43 (1992).
[56] A. K. Rajagopal, Phys. Rev. B **46**, 1224 (1992).
[57] A. MacDonald, H. Akera, and M. Norman, Aust. J. Phys. **46**, 333 (1993).
[58] J. Ryan and A. Rajagopal, J. Phys. Chem. Solids **54**, 1281 (1993).
[59] J. C. Ryan and A. K. Rajagopal, Phys. Rev. B **47**, 8843 (1993).
[60] M. R. Norman, A. H. MacDonald, and H. Akera, Phys. Rev. B **51**, 5927 (1995).
[61] M. M. Maśka, Phys. Rev. B **66**, 054533 (2002).
[62] P. Scherpelz, D. Wulin, B. c. v. Šopík, K. Levin, and A. K. Rajagopal, Phys. Rev. B **87**, 024516 (2013).
[63] S. Ran, I.-L. Liu, Y. S. Eo, D. J. Campbell, P. M. Neves, W. T. Fuhrman, S. R. Saha, C. Eckberg, H. Kim, D. Graf *et al.*, Nat. Phys. **15**, 1250 (2019).
[64] Y. Kim, A. C. Balram, T. Taniguchi, K. Watanabe, J. K. Jain, and J. H. Smet, Nat. Phys. **15**, 154 (2019).
[65] G. Chaudhary, A. H. MacDonald, and M. R. Norman, Phys. Rev. Res. **3**, 033260 (2021).
[66] J. Schirmer, C.-X. Liu, and J. K. Jain, Proc. Natl. Acad. Sci. USA **119**, e2202948119 (2022).
[67] J. Schirmer, J. K. Jain, and C. X. Liu, Phys. Rev. B **109**, 134518 (2024).
[68] X. G. Wen, Phys. Rev. Lett. **64**, 2206 (1990).
[69] Y. Hatsugai, P.-A. Bares, and X. G. Wen, Phys. Rev. Lett. **71**, 424 (1993).
[70] J. S. Birman, Commun. Pure Appl. Math. **22**, 41 (1969).
[71] T. Einarsson, Phys. Rev. Lett. **64**, 1995 (1990).
[72] X. G. Wen, Phys. Rev. B **41**, 12838 (1990).
[73] M. Oshikawa and T. Senthil, Phys. Rev. Lett. **96**, 060601 (2006).
[74] M. Sato, M. Kohmoto, and Y.-S. Wu, Phys. Rev. Lett. **97**, 010601 (2006).
[75] M. Oshikawa, Y. B. Kim, K. Shtengel, C. Nayak, and S. Tewari, Ann. Phys. (NY) **322**, 1477 (2007).
[76] F. D. M. Haldane, Phys. Rev. Lett. **55**, 2095 (1985).
[77] X. G. Wen and Q. Niu, Phys. Rev. B **41**, 9377 (1990).
[78] F. D. M. Haldane, Phys. Rev. Lett. **51**, 605 (1983).
[79] E. Rashba, Sov. Phys. Solid State **2**, 1109 (1960).
[80] Y. A. Bychkov and E. I. Rashba, J. Phys. C **17**, 6039 (1984).
[81] J. Schliemann, J. C. Egues, and D. Loss, Phys. Rev. B **67**, 085302 (2003).
[82] S.-Q. Shen, M. Ma, X. C. Xie, and F. C. Zhang, Phys. Rev. Lett. **92**, 256603 (2004).
[83] T. Ito, K. Nomura, and N. Shibata, J. Phys. Soc. Jpn. **81**, 034713 (2012).
[84] A. H. Castro Neto, F. Guinea, N. M. R. Peres, K. S. Novoselov, and A. K. Geim, Rev. Mod. Phys. **81**, 109 (2009).
[85] T. T. Wu and C. N. Yang, Nucl. Phys. B **107**, 365 (1976).
[86] T. T. Wu and C. N. Yang, Phys. Rev. D **16**, 1018 (1977).
[87] K. Nomura and A. H. MacDonald, Phys. Rev. Lett. **96**, 256602 (2006).
[88] M. O. Goerbig, R. Moessner, and B. Douçot, Phys. Rev. B **74**, 161407(R) (2006).
[89] V. M. Apalkov and T. Chakraborty, Phys. Rev. Lett. **97**, 126801 (2006).
[90] C. Tőke, P. E. Lammert, V. H. Crespi, and J. K. Jain, Phys. Rev. B **74**, 235417 (2006).
[91] C. Tőke and J. K. Jain, Phys. Rev. B **75**, 245440 (2007).
[92] A. C. Balram, C. Tőke, A. Wójs, and J. K. Jain, Phys. Rev. B **92**, 205120 (2015).
[93] A. Jellal, Nucl. Phys. B **804**, 361 (2008).
[94] M. Arciniaga and M. R. Peterson, Phys. Rev. B **94**, 035105 (2016).
[95] K. Hasebe, Int. J. Mod. Phys. A **31**, 1650117 (2016).
[96] K. Yonaga, K. Hasebe, and N. Shibata, Phys. Rev. B **93**, 235122 (2016).
[97] M. J. W. Dodgson, J. Phys. A: Math. Gen. **29**, 2499 (1996).
[98] M. J. W. Dodgson and M. A. Moore, Phys. Rev. B **55**, 3816 (1997).
[99] We have used the lowest Landau level vortex lattice as a simplest model, but this may not be enough for standard type-II superconductors [115]. This detailed study is left for the future.
[100] W. H. Kleiner, L. M. Roth, and S. H. Autler, Phys. Rev. **133**, A1226 (1964).
[101] J. J. Thomson, London Edinburgh Dublin Philos. Mag. J. Sci. **7**, 237 (1904).
[102] D. J. Wales and S. Ulker, Phys. Rev. B **74**, 212101 (2006).
[103] D. J. Wales, H. McKay, and E. L. Altschuler, Phys. Rev. B **79**, 224115 (2009).
[104] J. Zhao, Y. Zhang, and J. K. Jain, Phys. Rev. Lett. **121**, 116802 (2018).
[105] T. Ando, J. Phys. Soc. Jpn. **52**, 1740 (1983).
[106] I. Peschel, J. Phys. A: Math. Gen. **36**, L205 (2003).

[107] S.-A. Cheong and C. L. Henley, Phys. Rev. B **69**, 075111 (2004).
[108] S. Ryu and Y. Hatsugai, Phys. Rev. B **73**, 245115 (2006).
[109] H. Li and F. D. M. Haldane, Phys. Rev. Lett. **101**, 010504 (2008).
[110] I. D. Rodríguez and G. Sierra, Phys. Rev. B **80**, 153303 (2009).
[111] E. Prodan, T. L. Hughes, and B. A. Bernevig, Phys. Rev. Lett. **105**, 115501 (2010).
[112] A. Alexandradinata, T. L. Hughes, and B. A. Bernevig, Phys. Rev. B **84**, 195103 (2011).
[113] A. Sterdyniak, A. Chandran, N. Regnault, B. A. Bernevig, and P. Bonderson, Phys. Rev. B **85**, 125308 (2012).
[114] T. P. Oliveira, P. Ribeiro, and P. D. Sacramento, J. Phys.: Condens. Matter **26**, 425702 (2014).
[115] Z. Tešanović and P. D. Sacramento, Phys. Rev. Lett. **80**, 1521 (1998).